International Journal of Modern Physics B
Vol. 20, No. 8 (2006) 937–945
© World Scientific Publishing Company

World Scientific
www.worldscientific.com

TERAHERTZ RADIATION IN SUPERLATTICES IN MODERATE ELECTRIC FIELD

PENG HAN, KUI-JUAN JIN*, YUE-LIANG ZHOU and QING-LI ZHOU
Beijing National Laboratory for Condensed Matter Physics, Institute of Physics, Chinese Academy of Sciences, Beijing 100080, People's Republic of China
**kjjin@aphy.iphy.ac.cn*

K. HIRAKAWA
Institute of Industrial Science, University of Tokyo, 4-6-1 Komaba, Meguro-ku, Tokyo 153-8505, Japan

Received 24 June 2005

We have studied the terahertz (THz) radiation in superlattices (SLs) in moderate electric field region (between 12 kV/cm and 25 kV/cm) from both theoretical and experimental aspects in this work. The THz emission intensity has been calculated for three samples of GaAs/$Al_{0.3}Ga_{0.7}As$ SLs by using Kane model. The theoretical results show that the radiation intensity increases until the electric field F achieves a certain value between 14 kV/cm and 16 kV/cm for various samples, and then starts to roll off. The agreement of the calculated results with the experimental data demonstrates that the rolling of THz radiation intensity is due to the competition of field induced localization of wave functions and the increasing of the photon energy in THz radiation with increased electric fields. Furthermore, it is also shown that THz radiation intensity can be affected by the scattering of the randomly distributed Al atoms in the barriers.

Keywords: THz emission; superlattice; Kane model.

PACS numbers: 73.21.Cd, 73.40.-c, 78.47.+p

1. Introduction

Terahertz (THz) radiation, having a frequency between microwave and laser, has a number of highly interesting applications in biological imaging, surface chemistry, and high-field condensed matter studies.[1] There are many methods such as synchrotron radiation,[2] two-dimensional plasmon in single quantum well excited by femtosecond laser pluses[3,4] and vacuum-plasma interface driven by ultrashort intense laser pulses[5] to generate THz radiation. In 1993, THz emission was first observed from Bloch Oscillations (BOs) in superlattices (SLs) using time-resolved THz emission spectroscopy.[6] Till now, considerable effort in experimental[7–11] and theoretical aspects[12,13] has been made to investigate the topic of THz radiation in SLs. Recently, a joint theoretical and experimental study has been performed to give

the evidence that THz radiation observed in SLs is due to the BOs.[12] In addition, the broadening in the spectra of THz radiation and the oscillation in the intensity curve of the THz emission in the high electric field region have been concluded as the result of the interminiband Zener tunneling from both the experimental[9,10] and the theoretical aspects.[14]

In the case of low electric field region (F below 12 kV/cm), the Wannier Stark ladder (WSL) energy separation eFd (d: the SL period) is less than the level broadening due to scattering. Thus, the electromagnetic wave is emitted when electrons are accelerated in minibands. The THz radiation intensity has been calculated with a semiclassical Drude model in this region.[12] With the increase in electric fields, each miniband decomposes into a WSL of equal energy separation $\hbar\omega_B = eFd$, where ω_B is the BO frequency.[15] Therefore, the radiation intensity can be calculated with quantum theory using Wannier functions as basis functions. As the semiclassical approach is a method to describe electron movement in minibands and the Wannier functions offer an ideal tool for treating a system with WSLs,[12] these two models are good enough to treat the THz radiation when Zener tunneling is so small that it can be ignored except for the moderate electric field (between 12 kV/cm and 18 kV/cm).[12] Therefore, the search for a method to describe and to reveal the physics in THz radiation in SLs in such a crossover region in the moderate field continues.

Since the Kane model has been proposed to treat the one-dimensional Hamiltonian for an electron in a periodic potential system with applied static electric field F in 1959,[16] this model has become a good approximation in the treatment of SLs in electric fields without considering the coupling between different minibands.[7,15–22] In this model, the eigenvalues and the eigenfunctions of the Hamiltonian are composed of both the miniband term and the WSL term.[16,20] Therefore, we expect this model to be suitable for treating THz radiation when the minibands decompose into the WSLs in the moderate electric field region.

In this work, we calculated the total THz radiation intensity $I(F)$ in three samples of $GaAs/Al_{0.3}Ga_{0.7}As$ SLs with electric fields between $F = 12$ kV/cm and $F = 25$ kV/cm using the Kane model. Comparison of our theoretical results with the experimental data, a good agreement between our calculated THz radiation intensity and the measured THz intensity in this region has been obtained. These results reveal that the rolling of the radiation intensity in this crossover region is due to the competition of the localization of wave functions and the increase in the THz radiation photon energy $\hbar\omega_B = eFd$ with the increased electric fields. In addition, it is also shown that the scattering of the randomly distributed Al atoms in the barriers can affect the THz radiation intensity.

2. Experiment

The experimental setup, the measurement method, and the data analysis were given in details in Refs. 8–10. Here, we will only outline them briefly. The samples used

in the present study were GaAs/$Al_{0.3}Ga_{0.7}As$ SLs metal-intrinsic-n-type (m-i-n) diode structures. Three different undoped GaAs/$Al_{0.3}Ga_{0.7}As$ SLs samples (sample 1: 6.4 nm/0.56 nm with 73 periods, sample 2: 8.2 nm/0.8 nm with 55 periods, sample 3: 9.3 nm/1.3 nm with 47 periods) were grown on n^+-GaAs substrates by molecular beam epitaxy. The total thickness of the undoped SLs layer in each sample is 500 nm. The top contact of the samples was formed by depositing a semitransparent 4-nm-thick NiCr Schottky film, and the bottom ohmic contact was formed by annealing the Au–Ge–Ni alloy. By applying a bias voltage between the top and the bottom electrodes, we can tune an internal electric field F in the undoped SLs region.

Experiments were performed by using 100 fs laser pulses delivered from a mode-locked Al_2O_3:Ti laser. The laser pulses were loosely focused onto the sample surface. The pump photon energy was set to be 1.55 eV, which is close to the bottom of the miniband. When a femtosecond laser pulse excites the samples, electron-hole pairs are optically injectede into the miniband. Due to an applied electric field F, the carriers start drifting and THz radiation that is proportional to the carrier acceleration is emitted into free space. The generated THz emission was detected by a wideband Si bolometer operated at 4.2 K, whose bandwidth is up to 18 THz.

3. Theoretical Model

In this work, the x axis is regarded as the growth direction of the SLs, $d = a+b$ is the periodicity of the SLs where a is the width of the well and b is the barrier width. In addition, $V(x) = V(x + ld)$ is the one-dimensional lattice-periodic potential. Setting the zero reference energy at the bottom of GaAs conduction band edge, the barrier height is 250 meV. To model these SLs of finite length, we regard ld as the positions of the centers of the wells with $l = 1, 2, \ldots, m$, where m is the total number of the SLs' periods. The energy bands of these three samples are calculated with Kronig–Penney model shown in Fig. 1. The first miniband of sample 1 is between 18 meV and 114 meV, while the second miniband is between 150 meV and 445 meV. Thus, only the lower one third of the second miniband is under the potential barrier. The first miniband of sample 2 is between 19 meV and 69 meV, and the second miniband is between 107 meV and 270 meV. Hence, most of the second miniband lies below the potential barrier. The first miniband of sample 3 is between 21 meV and 49 meV, and the second miniband is between 100 meV and 199 meV. Therefore, both of these two minibands are below the potential barrier.

The Hamiltonian H of an electron with charge $-e$ in the SLs under an applied field F in the x axis of the SLs is expressed as

$$H = -\frac{\hbar^2}{2m^*}\frac{d^2}{dx^2} + V(x) + eFx \tag{1}$$

where, $\hbar$ is the reduced Planck constant and m^* is the effective mass of the electron. For $F = 0$, the eigenfunctions of the Hamiltonian in Eq. (1) can be written as

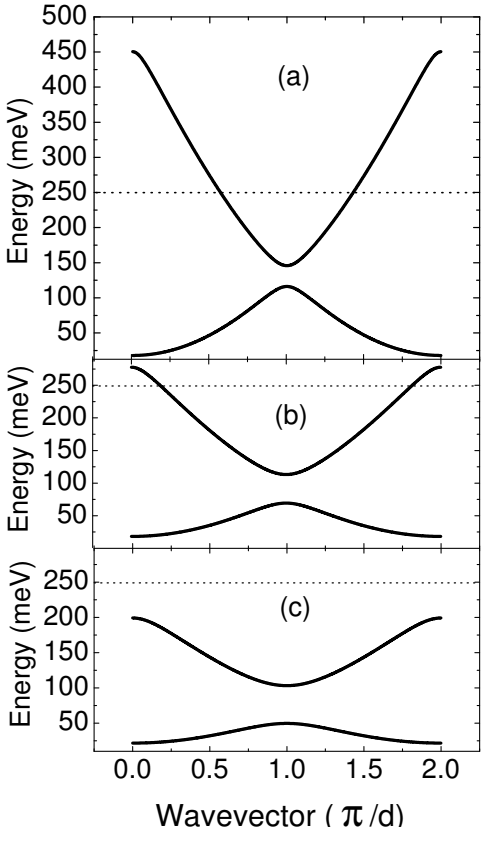

Fig. 1. The energy band of samples 1 (a), 2 (b) and 3 (c) obtained by Kronig–Penney model. The dotted lines denote the potential barrier.

Bloch functions $\phi_{nk}(x) = \frac{1}{\sqrt{2\pi}} e^{ikx} u_{nk}(x)$ where, n is the band index in our one-band system, k is the Bloch wave number and $u_{nk}(x)$ is the period part of Bloch function. For $F \neq 0$, the eigenfunctions of the Hamiltonian in Eq. (1) can be written as $\psi_n(x) = \sum_{k \in BZ} a_n(k) \phi_{nk}(x)$, which is the linear combination of the Bloch functions.

It is reasonable to ignore the coupling between various minibands in the field which we have considered.[12] The eigenvalues for the $a_n(k)$ can be solved by the following equation

$$\left[E_n(k) + ieF \frac{d}{dk} \right] a_n(k) + eF X_{nn}(k) a_n(k) = \epsilon a_n(k) \tag{2}$$

where $E_n(k)$ is the band energy of an electron in the periodic lattice without applied bias voltage F, and ϵ is the eigenvalue of the Hamiltonian in Eq. (1). The interminiband coupling parameter $X_{nn}(k)$ is defined as $X_{nn}(k) = \frac{i}{d} \int_{-d/2}^{+d/2} dx u_{nk}^*(x) \frac{du_{nk}(x)}{dk}$ and $X_{nn}(k)$ is the intraminiband coupling component.[16]

The eigenfunctions of Eq. (2) are known as the famous Kane functions, which have been presented elsewhere.[16,20] Then the eigenfunctions $\psi_{nl}(x) = \sum_{k\in BZ} a_{nl}(k)\phi_{nk}(x)$ and the eigenvalues $\epsilon_{nl} = \frac{d}{2\pi}\int_{-\pi/d}^{+\pi/d} dk'[E_n(k') + eFX_{nn}(k')] + eFdl$ of the Hamiltonian in Eq. (1) are obtained. The so-derived eigenvalues are composed of not only the miniband terms $E_n(k)$ and $eFX_{nn}(k)$, but also the energy separation term eFd which forms the WSL in the system.

Thus, the total radiation intensity $I(F)$ can be expressed as follows

$$I(F) = A\sum_{l'}(|l-l'|\hbar\omega_B)|\int_{SL} dx\psi^*_{nl}(x)x\psi_{nl'}(x)|^2 \tag{3}$$

where l' runs from 1 to m too. A is a field independent quantity, the value of which depends on the units used. It has been prove that under the condition where both the spontaneous and the stimulated emission are considered, the total intensity coefficient A is positive.[12] It is important to point out that though the summation runs over all pairs of WSL eigenfunctions in the electron miniband in Eq. (3), actually most of the radiation intensity is contributed by the electron transitions between two and three adjacent energy levels in the WSL because the overlap between localized eigenfunctions $\psi_{nl}(x)$ and $\psi_{nl'}(x)$ decreases rapidly as $|l-l'|$ increases.

4. Result and Discussion

The theoretical results and the experimental data of these three samples are shown in Figs. 2–4, respectively. In these figures, the solid lines represent the calculated results of Eq. (3) and the hollow circles denote the experimental data, respectively.

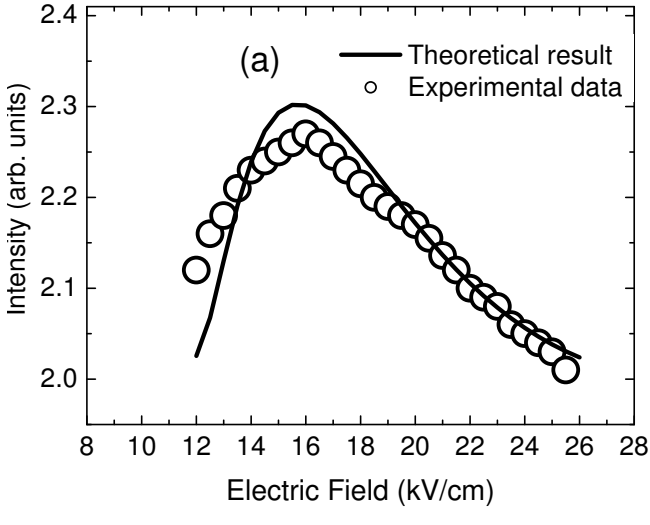

Fig. 2. The comparing between theoretical results and experimental data of sample 1. The solid line is calculated using Eq. (3), and the experimental data shown by hollow circles.

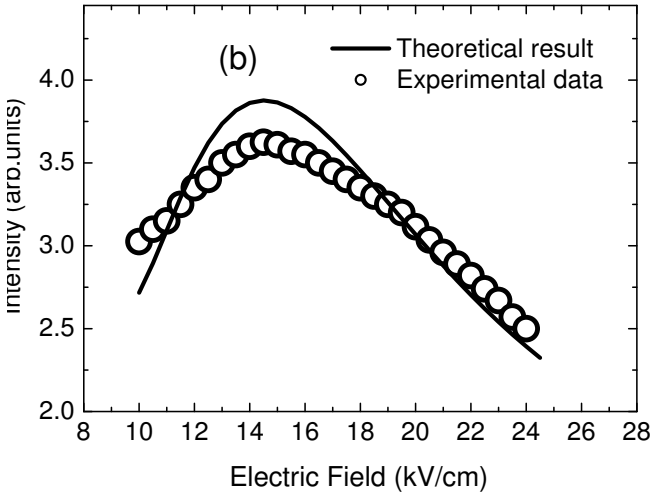

Fig. 3. The comparing between theoretical results and experimental data of sample 2. The solid line is calculated using Eq. (3), and the experimental data shown by hollow circles.

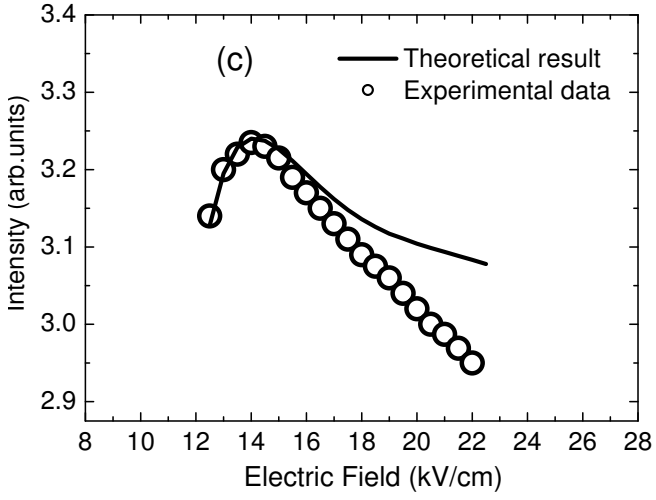

Fig. 4. The comparing between theoretical results and experimental data of sample 3. The solid line is calculated using Eq. (3), and the experimental data shown by hollow circles.

It can be seen that the radiation intensity $I(F)$ increases with F in the low field region, then $I(F)$ achieves its maximum with F at a certain value between 14 kV/cm and 16 kV/cm for various samples. With the further increased electric field, the radiation intensity starts to roll off and decreases with F in the electric field region which we have considered. Comparing the theoretical results we calculated with the experimental data in these three figures, it can be seen that the calculated curves agree well with the measured data.

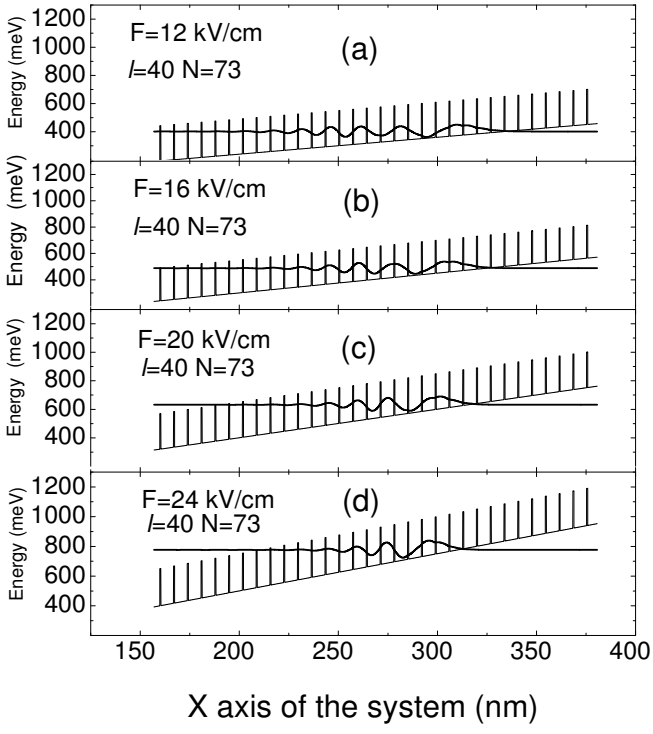

Fig. 5. (a) is the 40th wave function of sample 1 with $F = 12$ kV/cm, (b) is the 40th wave function of sample 1 with $F = 16$ kV/cm, (c) is the 40th wave function of sample 1 with $F = 20$ kV/cm, (d) is the 40th wave function of sample 1 with $F = 24$ kV/cm.

The process of radiation intensity starting to roll off in this moderate field region can be expressed as follows. The total radiation intensity $I(F)$ is determined by two parts, one is the THz radiation photon energy $\hbar\omega_B = eFd$, the other is the coupling between two wave functions. The former increases with F linearly and the latter decreases with F. The wave functions of sample 1 with different electric fields are plotted in Fig. 5, where wave functions are partly localized but still extending into several neighboring wells. Furthermore, the extension of the wave function decreases with the increase in electric fields. Thus, the space overlap of the two neighboring wave functions decreases with the increase in electric fields. Therefore, the competition of the localization of wave functions and the increased photon energy $\hbar\omega_B$ resulted from the increased electric field is the reason for THz radiation starting to roll off in this crossover region.

We noticed that the theoretical results and the experimental data of sample 3 in Fig. 4 do not agree as good as other samples in the high field region (above 17 kV/cm). This may be attributed to the damping of BOs by scattering of the randomly distributed Al atoms in the barriers. In the SL samples used in the present study, Al atoms are randomly distributed in the barriers and stochastic fluctuation

of the δ-function-like potential of Al atoms in the barriers scatters the tunneling electrons. So the damping of BOs increases with the number of Al atoms per unit volume. This scattering mechanism of BOs in SLs is known as alloy disorder scattering.[23] To compare the effects of the alloy disorder scattering of various samples, we define $r = b/d$ to describe the rate of Al atom in a periodicity of SLs. The r for samples 1, 2 and 3 are 0.0805, 0.0889, and 0.1226, respectively. Thus, the damping of BOs by the alloy disorder scattering in sample 3 is much larger than the other two samples. This also explains why the agreement of sample 1 is slightly better than that of sample 2.

5. Summary and Conclusion

We have calculated the THz radiation intensity in SLs with electric field F between 12 kV/cm and 25 kV/cm using the Kane model. The agreement between theoretical results and the experimental data (expressed in arbitrary units) demonstrates that the rolling of the radiation intensity in this crossover region is due to the competition of the localization of wave functions and the increase in THz radiation photon energy $\hbar\omega_B$ with the increased electric fields. In addition, the results also demonstrate that the THz radiation intensity can be affected by the scattering of the randomly distributed Al atoms in the barriers.

Acknowledgment

We gratefully acknowledge the financial support from the National Natural Science Foundation of China (No. 60321003). This work was also supported by the SIDA-Swedish Research Links (Grant No. 348-2002-6935).

References

1. D. D. Arnone, C. M. Ciesla and M. Pepper, *Phys. World* **13**, 35 (2000).
2. T. Nakazato, M. Oyamada, N. Niimura, S. Urasawa, O. Konno, A. Kagaya, R. Kato, T. Kamiyama and Y. Torizuka, *Phys. Rev. Lett.* **63**, 1245 (1998).
3. N. Sekine, K. Yamanaka, K. Hirakawa, M. Voßebürger, P. Haring-Bolivar and H. Kurz, *Appl. Phys. Lett.* **74**, 1006 (1999).
4. N. Sekine, K. Hirakawa, M. Voßebürger, P. Haring-Bolivar and H. Kurz, *Phys. Rev. B* **64**, 201 323 (2001).
5. Z. M. Sheng, H. C. Wu, K. Li and J. Zhang, *Phys. Rev. E* **69**, 025 401 (2004).
6. C. Waschke, H. G. Roskos, R. Schwedler, K. Leo, H. Kurz and K. Köhler, *Phys. Rev. Lett.* **70**, 3319 (1993).
7. K. Leo, *High-Field Transport in Semiconductor Superlattices* (Springer-Verlag, Berlin Heidelberg, 2003).
8. Y. Shimada, K. Hirakawa and S.-W. Lee, *Appl. Phys. Lett.* **81**, 1642 (2002).
9. Y. Shimada, K. Hirakawa, M. Odnoblioudov and K. A. Chao, *Phys. Rev. Lett.* **90**, 046 806 (2003).
10. Y. Shimada, N. Sekine and K. Hirakawa, *Appl. Phys. Lett.* **84**, 4926 (2004).
11. K. Leo, P. Haring-Bolivar, F. Brüggemann, R. Schwedler and K. Köhler, *Solid State Commun.* **84**, 943 (1992).

12. K.-J. Jin, M. Odnoblyudov, Y. Shimada, K. Hirakawa and K. A. Chao, *Phys. Rev. B* **68**, 153 315 (2003).
13. J. Bleuse, G. Bastard and P. Voisin, *Phys. Rev. Lett.* **60**, 220 (1988).
14. P. Han, K.-J. Jin, Y. L. Zhou, Q.-L. Zhou, H.-B. Lu, D.-Y. Guan and G.-Z. Yang, *Europhys. Lett.* **72**, 1011 (2005).
15. G. H. Wannier, *Rev. Mod. Phys.* **34**, 645 (1962).
16. E. O. Kane, *J. Phys. Chem. Solids* **12**, 181 (1959).
17. M. M. Dignam, J. E. Sipe and J. Shah, *Phys. Rev. B* **49**, 10 502 (1994).
18. D. M. Whittaker, *Europhys. Lett.* **31**, 55 (1995).
19. N. Linder, *Phys. Rev. B* **55**, 13 664 (1997).
20. S. Glutsch, *Phys. Rev. B* **69**, 235 317 (2004).
21. S. Glutsch and F. Bechstedt, *Phys. Rev. B* **60**, 16 584 (1999).
22. S. Glutsch, F. Bechstedt, B. Rosam and K. Leo, *Phys. Rev. B* **63**, 085 307 (2001).
23. N. Sekine, Y. Shimada and K. Hirakawa, *Appl. Phys. Lett.* **83** 4794 (2003).